Proceedings of the XVII ECSMGE-2019
Geotechnical Engineering foundation of the future
ISBN 978-9935-9436-1-3

doi: 10.32075/17ECSMGE-2019-0959

XVII European Conference
ECSMGE 2019
Reykjavik
on Soil Mechanics
and Geotechnical Engineering

On the incremental behaviour of sands at high stresses

Sur le comportement incrémental des sables sous fortes contraintes

M. O. Ciantia
University of Dundee, School of Science and Engineering, Dundee, UK
M. Arroyo, A. Gens
Universitat Politècnica de Catalunya, Dept. Civil and Environmental Engineering, Barcelona, Spain

ABSTRACT: The mechanical behaviour of granular materials is characterized by strong non-linearity and irreversibility. In particular, particle breakage will induce additional plastic deformations beyond those which might be expected for a rigid particle assumption. When defining a constitutive model, experimental data on the nature of the incremental response of the material is desirable. However, the experiments are very challenging and therefore test simulations using the discrete element method (DEM) are very useful. In this work, the incremental behaviour of crushable granular soils is investigated using the DEM by simulating 3D axisymmetric stress probes experiments on a Fontainebleau sand analogue. Particle breakage is permitted and the initial high stress condition is such that crushing will occur along some of the loading directions. The results show that particle crushing induces a change in the direction of the plastic flow and that this direction is independent of the loading path.

RÉSUMÉ: Le comportement mécanique des matériaux granulaires est caractérisé par une forte non-linéarité et une irréversibilité. En particulier, la rupture des particules induira des déformations plastiques supplémentaires allant au-delà de celles auxquelles on pourrait s'attendre pour une hypothèse de particule rigide. Lors de la définition d'un modèle constitutif, des données expérimentales sur la nature de la réponse incrémentielle du matériau sont souhaitables. Cependant il est très difficile de reproduire un ensemble d'échantillons identiques à utiliser dans une étude paramétrique expérimentale. Les simulations de test utilisant la méthode des éléments discrets (DEM) sont donc très utiles. Dans ce travail, le comportement incrémental des sols granulaires déformables est étudié à l'aide du DEM en simulant des expériences de sondes de contrainte axisymétriques 3D sur un analogue de sable de Fontainebleau. La rupture de particules est autorisée et la condition initiale de fortes contraintes est telle que des écrasements se produiront dans certaines directions de chargement. Les résultats montrent que le broyage de particules induit un changement de direction du flux de plastique et que cette direction est indépendante du chemin de chargement.

Keywords: Distinct element method; granular materials; incremental non linearity; crushing; response envelops;

1 INTRODUCTION

Grain fragmentation is significant for several important geotechnical problems, such as side friction on driven piles and railway ballast durability. For this reason particle breakage is now featured into constitutive models for soils (Kikumoto et al., 2010; Li et al., 2015). Those models are supported by experimental laboratory investigations (Coop et al., 2004; Donohue et al., 2009; Lade et al., 1996). DEM models of crushable soils (Cheng et al., 2004; Ciantia et al., 2014a, 2015, 2016a) can also provide ancillary experiments to supplement expensive and/or difficult laboratory tests.

We focus on the deformation response to a series of "small" increments in stress (probes) that, starting from a unique initial state, point in varying directions in stress space. This incremental response provides important information for constitutive models.

Measuring incremental responses in the laboratory is difficult (Costanzo et al., 2006; Danne and Hettler, 2015), because of the highly accurate strain measurements required and the need to test several identical samples (one for each probe). For this reason DEM models have been used to study the incremental behaviour of granular materials (Bardet, 1994; Calvetti et al., 2003; Thornton and Zhang, 2010; Wan and Pinheiro, 2014). Ciantia et al., (2016b) extended this technique to the case of crushable soils.

In this contribution the direction and magnitude of plastic flow when grain crushing is present is considered. Incremental probes are systematically applied to explore the effect of stress obliquity and grading index on the plastic flow pattern on triaxial conditions.

2 DEM MODEL DESCRIPTION

2.1 Particle failure criterion & calibration

The modelling approach adopted was outlined by (Ciantia et al., 2015). Spherical particles whose rotation was inhibited were used to capture the rotational resistance that exists between non-spherical grains (Ciantia et al., 2014b, 2019b). The contact model follows uses a simplified Hertz-Mindlin formulation and Coulomb friction. The limit criterion at which breakage is activated for a given particle was formulated following (Russell and Muir Wood, 2009). A particle breaks if the force F, at any of its contacts is such that

$$F = \sigma_{lim} \cdot A_F \tag{1}$$

where σ_{lim} is the limit strength of the material and A_F is the contact area. To incorporate the natural material variability into the model, the limit strength, σ_{lim}, is assumed to be normally distributed for a given sphere size. The coefficient of variation of the distribution, *var*, is taken to be a material parameter.

$$\sigma_{lim} = \sigma_{lim0} \cdot (d/d_0)^{-3/m} \tag{2}$$

Once the limit condition is reached, a particle, modelled as a sphere in the PFC DEM code used (Itasca, 2017), will split into smaller inscribed tangent spheres. Using a simplified Hertz-Mindlin to describe the contact area eq. (1) results

$$F \leq \left\{ \sigma_{lim} \left(\frac{d}{d_0}\right)^{\frac{-3}{m}} \pi \left[\frac{3}{4} \frac{\left(\frac{1-\nu_1^2}{E_1}+\frac{1-\nu_2^2}{E_2}\right)}{\left(\frac{1}{r_1}+\frac{1}{r_2}\right)} \right]^{\frac{2}{3}} \right\}^3 \tag{3}$$

where r_1 and r_2 are the radii of the contacting spheres and E_i, ν_i are the Young's Moduli and Poisson's ratio respectively. Note that this breakage criterion does not involve exclusively the maximum force on the particle: there is a strong inbuilt dependency on the characteristics of the contacting particles Full details of the model are reported in (Ciantia et al., 2015). In this work, a cubic numerical specimen with a side length of 4mm is filled with about 10,000 randomly assembled rigid particles with a grain size distribution corresponding closely to that of Fontainebleau sand (Yang et al., 2010) with particle diameters ranging from 0.1 to 0.4 mm. Gravity was set to zero and the specimen boundaries were defined using smooth "wall" elements. Target stress values were attained by using a servo-control to adjust the wall positions. As the rigid boundaries were smooth the principal axes of stress and strain are coincident with the cube axes. The principal strains were calculated directly from the wall displacements, while the corresponding principal stresses were obtained from the boundary forces. The contact law parameters were calibrated by simulating drained triaxial compression of dense and loose specimens under 100 kPa

confinement (Figure 1a). The particle failure criterion parameters were calibrated simulating a one dimensional high pressure compression test (Figure 1b) by capturing the apparent yield point of the loading curve (Cheng et al., 2004). The calibrated model parameters are summarized in Table 1.

Table 1. DEM input parameters for simulation

d_{50} mm	μ rad	G GPa	ν –	$\sigma_{lim,0}$ GPa	m -	d_0 mm	var -
0.21	0.27	3	0.3	5	10	2	1

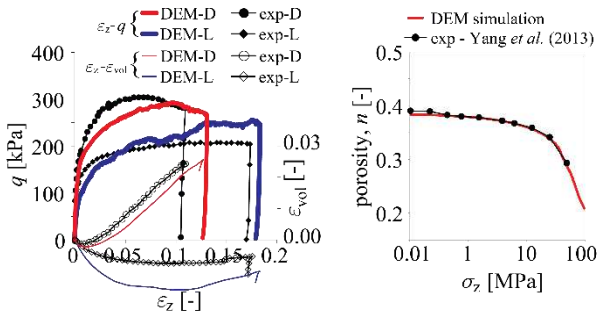

a) b)

Figure 1. DEM and experimental curves of (a) drained triaxial compression and (b) oedometric compression tests.

2.2 Initial states

Ciantia *et al.* (2019a) investigated the incremental behaviour of a virtual analogue of Fontainebleau sand starting from various (14) initial states in the *triaxial* (q/p') plane. In this work a point (Point A) lying on a constant p' triaxial compression stress path with stress ratio, $\eta = q/p'$, of 0.5 was selected for probing. Figure 2 shows the stress path and the initial conditions of Point A in the compression plane while Table 2 summarizes its initial conditions.

Table 2. Initial states

State ID	η	I_G [-]	p' [MPa]	q [MPa]	e [-]
Point A	0.5	0.808	52.4	26.2	0.278

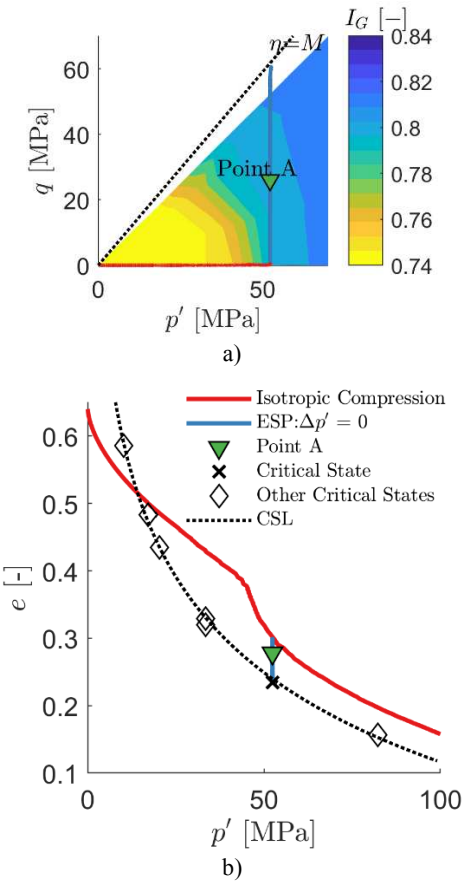

a) b)

Figure 2. Point A in the triaxial plane and grading index contours (a) and in the compression plane with indication of isotropic compression path and critical state line (b).

2.3 Stress probing

For axisymmetric (triaxial) loading, the number of independent stress and strain variables reduces to two, and a convenient graphical representation can be given in the Rendulic plane (Figure 3a). The stress probe magnitude is then

$$\|\Delta\boldsymbol{\sigma}'\| = \sqrt{\Delta\boldsymbol{\sigma}' \cdot \Delta\boldsymbol{\sigma}'} = \sqrt{2\Delta\boldsymbol{\sigma}_x'^{\,2} + \Delta\boldsymbol{\sigma}_z'^{\,2}} \quad (4)$$

where σ'_z is the vertical stress, and the two horizontal stresses (σ'_x and σ'_y) are equal for this axisymmetric case. The stress probe magnitudes used here were 1% of the current principal stress.

The stress probe direction is defined by the angle $\alpha_{\Delta\sigma}$ between the horizontal axis and the stress increment vector as indicated in Figure 3a. The response is depicted using the incremental strain response envelope (RE) (Figure 3b). The direction of strain increment is defined by the angle $\alpha_{\Delta\varepsilon}$, between the horizontal axis and the strain increment vector.

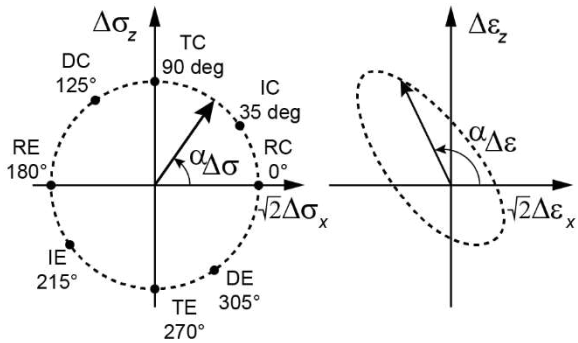

(a) (b)

Figure 3. Stress probes (a) and Response envelope to stress probes (b)

In this work, strain responses for 36 probes with 10° $\alpha_{\Delta\sigma}$ incremental spacing for state A in Figure 1b were performed. As detailed in Ciantia et al 2016a, the incremental deformation observed, $\Delta\boldsymbol{\varepsilon}$, can be decomposed into a reversible ("elastic") part $\Delta\boldsymbol{\varepsilon}^e$, and two irreversible parts: $\Delta\boldsymbol{\varepsilon}^{pu}$ ("plastic-uncrushable"), the irreversible strain increment in the case where no crushing occurs, and $\Delta\boldsymbol{\varepsilon}^{pc}$, the crushing induced plastic strain increments so that

$$\Delta\boldsymbol{\varepsilon} = \Delta\boldsymbol{\varepsilon}^{\boldsymbol{e}} + \Delta\boldsymbol{\varepsilon}^{\boldsymbol{pu}} + \Delta\boldsymbol{\varepsilon}^{\boldsymbol{pc}}. \quad (5)$$

To achieve this decomposition three simulations were run for each stress probe. The first simulation used the crushable DEM model described above to measure $\Delta\boldsymbol{\varepsilon}$. In the second simulation all the mechanisms responsible for plasticity (interparticle sliding, opening of contacts and particle crushing) were inhibited to give $\Delta\boldsymbol{\varepsilon}^e$. In the final simulation only crushing was inhibited to measure $\Delta\boldsymbol{\varepsilon}^e+\Delta\boldsymbol{\varepsilon}^{pu}$.

3 RESULTS

3.1 Macro scale

The complete set of macro scale results in terms of response envelopes and plastic flow evolution confirm the preliminary, low resolution, observations by Ciantia et al., (2016b). At each probing point the two plastic strain components ($\Delta\boldsymbol{\varepsilon}^{pu}$ and $\Delta\boldsymbol{\varepsilon}^{pc}$) have unique flow directions. Both plastic flow components become more deviatoric as η increases. Whenever both the components appear $\Delta\boldsymbol{\varepsilon}^{pc}$ is always more volumetric than $\Delta\boldsymbol{\varepsilon}^{pu}$. The variation in the magnitude of the plastic deformations ($\Delta\boldsymbol{\varepsilon}^{pu}$ and $\Delta\boldsymbol{\varepsilon}^{pc}$) with $\alpha_{\Delta\varepsilon}$ can be described by two distinct cosine shaped curves and the maxima of these curves coincide with the one of their corresponding flow (non-associated type of flow).

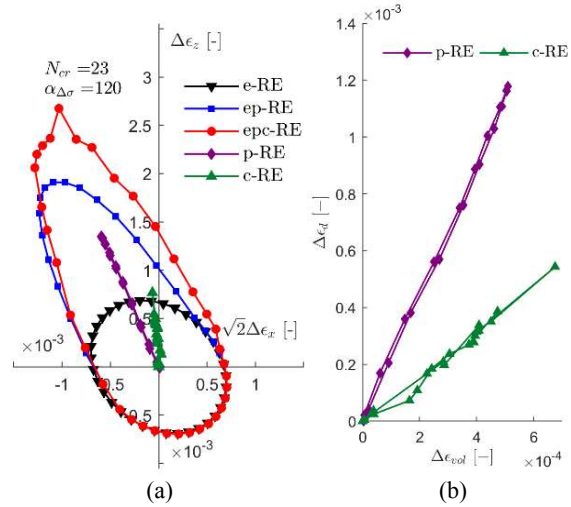

(a) (b)

Figure 4. Strain response envelopes (RE) in the Rendulic (a) and deviatoric (b) planes

Figure 4 summarizes the macroscopic results of the probes performed starting from the *B075* state for the η=0.75 radial compression stress paths. In Figure 4a, the elastic (*e*), elasto-plastic (*e-p*), elasto-plastic-crushable (*e-p-c*), plastic-uncrushable (*p*) and plastic-crushable (*c*) response envelopes (REs) are represented in the Rendulic plane. The orientation and number of crushed particles on the *e-p-c* RE for the probe

giving the most crushing events (N_{cr}) is indicated. The right column of Figure 4 reports the (p) and (c) RE in the triaxial plane and shows that the crushing RE is more volumetric than the non-crushing response. Figure 5 summarizes the plastic flow analyses of the of the stress probe results and shows that both plastic mechanisms are well interpolated by cosine shaped curves. The plastic deformation direction is, independent of the loading direction and, as for a two-mechanism plasticity framework, distinct for each plastic mechanism: 112° for the plastic-uncrushable case and 94° for the plastic-crushable case.

In a single mechanism plasticity framework (single yielding surface), the plastic strains are defined by a classical flow rule (Tamagnini and Ciantia, 2016)

$$\dot{\boldsymbol{\varepsilon}}^p = \dot{\lambda}\boldsymbol{n_g} \;;\; \boldsymbol{n_g} = \frac{1}{g^*}\frac{\partial g}{\partial \boldsymbol{\sigma}} \;;\; g^* = \left\|\frac{\partial g}{\partial \boldsymbol{\sigma}}\right\| \quad (5)$$

where $\boldsymbol{n}_g$ defines the plastic flow direction as the normalized gradient of a scalar plastic potential $\boldsymbol{g}$ and $\dot{\lambda} \geq 0$ is the plastic multiplayer. The evolution of internal variables is described by a hardening law

$$\dot{\boldsymbol{q}} = \dot{\lambda}\boldsymbol{h}(\boldsymbol{\sigma}, \boldsymbol{q}) \quad (6)$$

where $\boldsymbol{h}$ is a suitable hardening function. Subjecting the plastic multiplier in (5) and (6) to the Kuhn Tucker complementary conditions (Simo and Hughes, 1998) and imposing consistency for states on the yield surface $f(\boldsymbol{\sigma},\boldsymbol{q})$ gives

$$\dot{\lambda} = \frac{1}{H}\boldsymbol{n_f}\dot{\boldsymbol{\sigma}} \;;\; \boldsymbol{n_f} = \frac{1}{f^*}\frac{\partial f}{\partial \boldsymbol{\sigma}} \;;\; f^* = \left\|\frac{\partial f}{\partial \boldsymbol{\sigma}}\right\| \quad (7)$$

where $H = -\frac{1}{f^*}\frac{\partial f}{\partial \boldsymbol{q}}\boldsymbol{h}$ and therefore

$$\|\dot{\boldsymbol{\varepsilon}}^p\| = \frac{1}{H}\boldsymbol{n_f}\dot{\boldsymbol{\sigma}} \quad (8)$$

The magnitude of the plastic flow is hence given by a cosine shaped curve (an inner product) that is maximum when the stress increment is collinear with $\boldsymbol{n}_f$ (Figure 6). In principle, this direction of maximum plastic deformation ($\alpha_{\boldsymbol{nf}}$) may coincide or not with the plastic flow direction ($\alpha_{\boldsymbol{ng}}$). The latter case corresponds to non-associated behaviour, the former to associated behaviour.

In a two-mechanism plasticity framework there are two distinct yielding surfaces (one for each mechanism), leading to a non-unique plastic flow direction and to a plastic deformation obtained as the sum of two cosine shaped curves (Figure 6). As shown in Figure 5 the data presented here can be represented using a two mechanism non-associated plasticity framework. The plastic uncrushable and plastic crush deformations have a distinct yield surface $\alpha_{\boldsymbol{nf}}^{pu} \neq \alpha_{\boldsymbol{nf}}^{pc}$ and for each plastic mechanism (plastic-uncrushable and plastic-crush) the yield surface does not coincide with the plastic potential: $\alpha_{\boldsymbol{nf}}^{pu} \neq \alpha_{\boldsymbol{ng}}^{pu}$ and $\alpha_{\boldsymbol{nf}}^{pc} \neq \alpha_{\boldsymbol{ng}}^{pc}$.

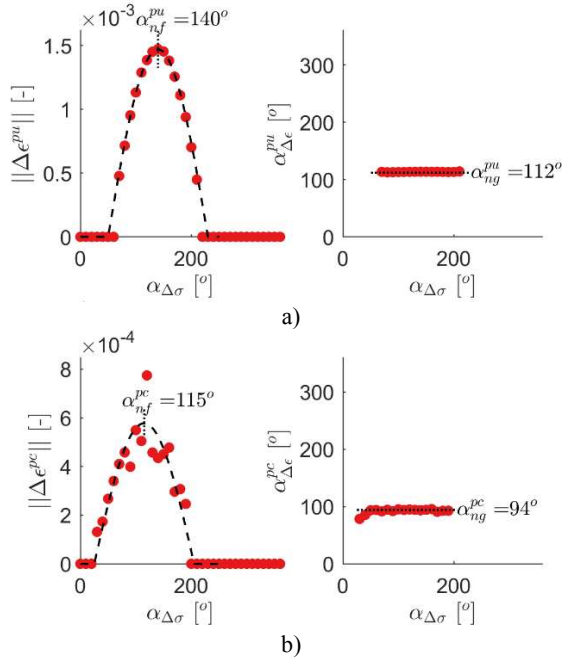

Figure 5. Plastic-uncrushable (a) and plastic crushable (b) plastic flow analysis.

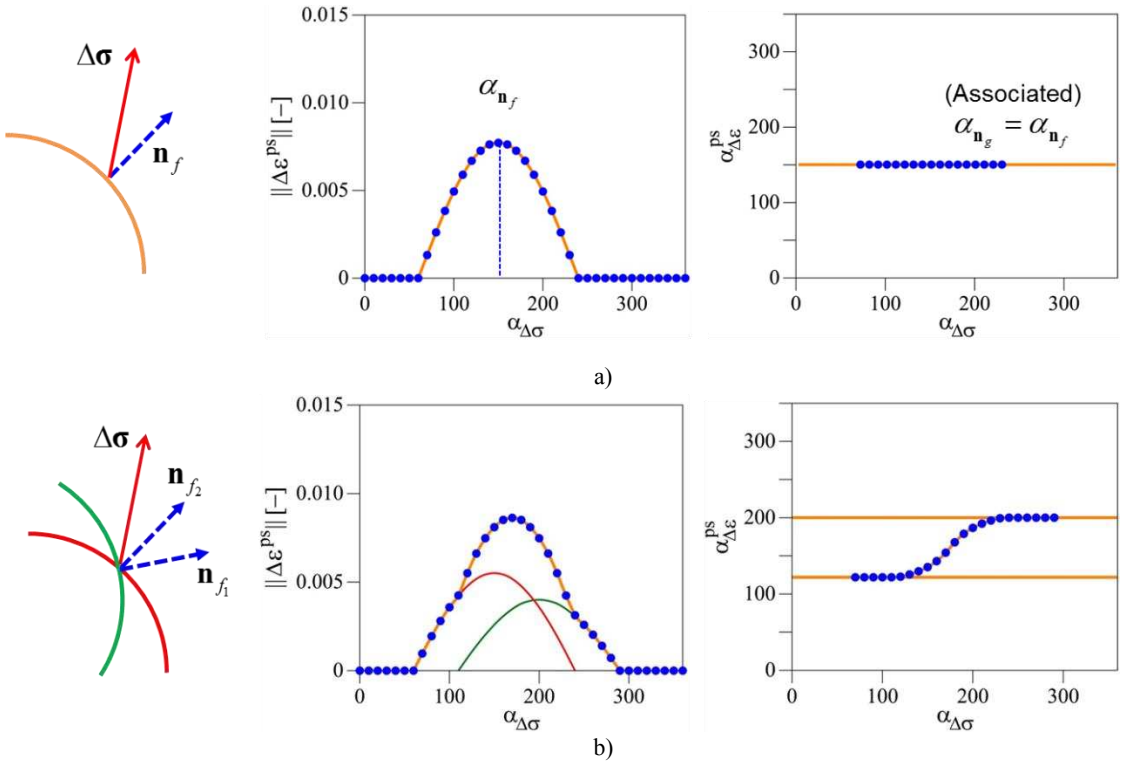

Figure 6 (a) Single mechanism and (b) double mechanism plasticity irreversible incremental response framework.

3.2 Micro scale

Microscale variables can offer further insight on the mechanisms involved. In particular following Calvetti et al., (2003) we analyse the effect of particle crushing at the contact level, by evaluating how close to sliding is each contact

$$\eta_\mu = \frac{f_t}{\mu f_n}. \tag{9}$$

For sliding contacts η_μ=1 when slip occurs, otherwise η_μ<1. In the elastic parallel probes, interparticle sliding is inhibited and η_μ can exceed unity. The magnitude of shear force exceeding the Coulomb limiting force (μf_n) represents a plastic shear overshoot only possible because contact-sliding was inhibited and is defined as

$$\Delta f^p = f_t - \mu f_n. \tag{10}$$

The η_μ computed for each contact at the end of each stress probe, for both the elasto-plastic probes and the elastic probes (in which interparticle slip is inhibited) is given in Figure 7. In the elastic probes, a plastic shear overshoot develops at the contacts that will slip in the corresponding elastoplastic (e-p) probe.

A cumulative plastic shear overshoot may be calculated by summation over a certain subset contacts (N_c):

$$\Delta F^p = \sum_1^{N_c} \Delta f^p \tag{11}$$

Using a sequential probe approach (see Ciantia et al., 2019) the contacts where slip is induced solely by particle crushing may be identified. In Figure 8 the cumulative plastic overshoot ΔF^p is represented for that contact subset as function of

the loading direction $\alpha_{\Delta\sigma}$. It appears that the data can be fitted by a half cosine shaped function that has a maximum for the same macroscopic loading direction denoted as α_{nf}^{pc} (see Figure 5).

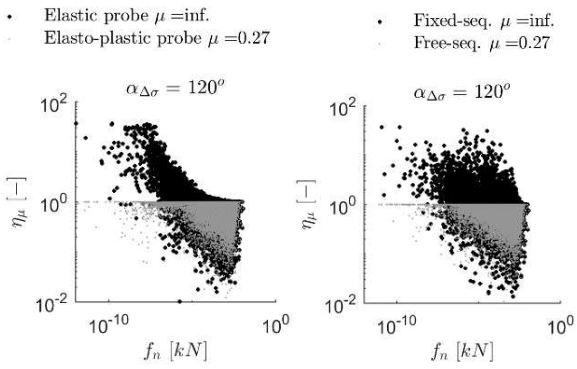

Figure 7 Mobilized interparticle friction as a function of normal contact force for the a) Elastic and elastoplastic and b) free and fixed sequential probes.

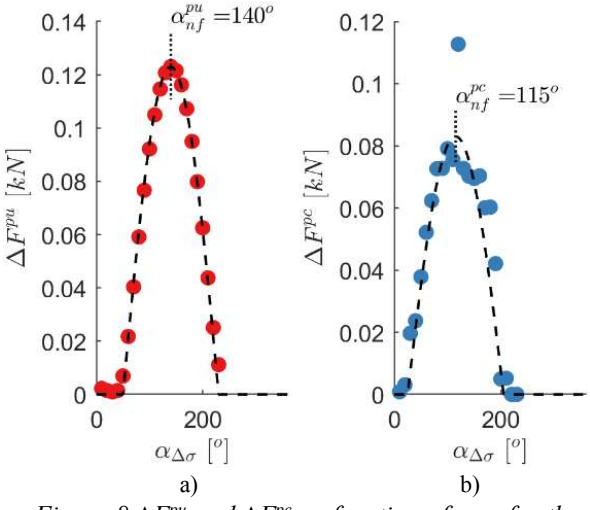

Figure 8 ΔF^{pu} and ΔF^{pc} as function of $\alpha_{\Delta\sigma}$, for the slipping contacts.

4 CONCLUSIONS

The incremental response of a crushable sand analogue has been examined using DEM to show that the inclusion of crushing as another source of plasticity in granular materials changes the direction of plastic flow, introducing more contraction.

The direction of plastic flow induced by crushing is independent of the loading direction and the variation in the magnitude of plastic strains (crushable and uncrushable) with loading direction is well approximated by a half cosine shaped function. Such response had already been identified experimentally at low confinement pressures (uncrushable regime) on Ottawa sand (Anandarajah et al., 1995) and on clays (Lewin and Burland, 1970).

The results of these extensive DEM triaxial stress-probe virtual experiments suggest that the inclusion of crushing as another source of plasticity is well described by a two-mechanism plasticity framework.

A detailed analysis of the sliding contacts unveils that both crushable and uncrushable macroscale incremental response of is linked to the evolution of the microstructure in terms of the cumulative plastic overshoot ΔF^p.

5 ACKNOWLEDGEMENTS

The BGA and the ISSMGE are gratefully acknowledged for having covered part of the conference fees of the first author.

6 REFERENCES

Anandarajah, A., Sobhan, K., Kuganenthira, N., 1995. Incremental Stress-Strain Behavior of Granular Soil. *J. Geotech. Eng*. **121**, 57–68.

Bardet, J.P., 1994. Numerical simulations of the incremental responses of idealized granular materials. *Int. J. Plast*. **10**, 879–908.

Calvetti, F., Tamagnini, C., Viggiani, G., 2003. Micromechanical inspection of constitutive modelling. In: Hevelius (Ed.), Constitutive Modelling and Analysis of Boundary Value Problems in Geotechnical Engineering. Benevento, pp. 187–216.

Cheng, Y.P., Bolton, M.D., Nakata, Y., 2004. Crushing and plastic deformation of soils simulated using DEM. *Géotechnique* **54**, 131–

141.

Ciantia, M.O., Arroyo, M., Gens, A., Calvetti, F., 2014a. Particle failure in DEM models of crushable soil response. In: Hicks, M.A., Brinkgreve, R.B.J., Rohe, A. (Eds.), Numerical Methods in Geotechnical Engineering. CRC Press/Balkema, Leiden, the Netherlands, pp. 345–35

Ciantia, M.O., Arroyo, M., Butlanska, J., Gens, A., 2014b. DEM modelling of a double porosity crushable granular material. Proc. Int. Symp. Geomech. from Micro to Macro 269–274.

Ciantia, M.O., Arroyo, M., Butlanska, J., Gens, A., 2016a. DEM modelling of cone penetration tests in a double-porosity crushable granular material. *Comput. Geotech*. **73**, 109–127.

Ciantia, M.O., Arroyo, M., Calvetti, F., Gens, A., 2015. An approach to enhance efficiency of DEM modelling of soils with crushable grains. *Géotechnique* **65**, 91–110.

Ciantia, M.O., Arroyo, M., Calvetti, F., Gens, A., 2016b. A numerical investigation of the incremental behavior of crushable granular soils. *Int. J. Numer. Anal. Methods Geomech*. **40**, 1773–1798.

Ciantia, M., Arroyo, M., O'Sullivan, C., Gens, A., Liu, T., 2019a. Grading evolution and critical state in a discrete numerical model of Fontainebleau sand. *Géotechnique* **69**:1, 1-15.

Ciantia, M.O., Arroyo, M., O'Sullivan, C., Gens, A., 2019b. Micromechanical Inspection of Incremental Behaviour of Crushable Soils. *Acta Geotech*. (Under review)

Coop, M.R., Sorensen, K.K., Bodas Freitas, T., Georgoutsos, G., 2004. Particle breakage during shearing of a carbonate sand. *Géotechnique* **54**, 157–163.

Costanzo, D., Viggiani, G., Tamagnini, C., 2006. Directional response of a reconstituted fine-grained soil—Part I: experimental investigation. *Int. J. Numer. Anal. Methods Geomech*. **30**, 1283–1301.

Danne, S., Hettler, A., 2015. Experimental Strain Response-Envelopes of Granular Materials for Monotonous and Low-Cycle Loading Processes. In: Triantafyllidis T. (eds) Holistic Simulation of Geotechnical Installation Processes. vol 77. Springer, Cham.

Donohue, S., O'sullivan, C., Long, M., 2009. Particle breakage during cyclic triaxial loading of a carbonate sand. *Géotechnique* **59**, 477–482.

Itasca, 2017. PFC *Particle Flow Code*, Ver. 5.0.

Kikumoto, M., Wood, D.M., Russell, A., 2010. Particle Crushing and Deformation Behaviour. *Soils Found*. **50**, 547–563.

Lade, P. V., Yamamuro, J.A., Bopp, P.A., 1996. Significance of Particle Crushing in Granular Materials. *J. Geotech. Eng*. **122**, 309–316.

Lewin, P.I., Burland, J.B., 1970. Stress-Probe Experiments on Saturated Normally Consolidated Clay. *Géotechnique* **20**, 38–56

Li, G., Liu, Y. J., Dano, C., Hicher, P.Y., 2015. Grading-Dependent Behavior of Granular Materials: From Discrete to Continuous Modeling. *J. Eng. Mech*. **141**, 04014172.

Russell, A.R., Muir Wood, D., 2009. Point load tests and strength measurements for brittle spheres. *Int. J. Rock Mech. Min. Sci*. **46**, 272–280.

Seif El Dine, B., Dupla, J. C., Frank, R., Canou, J. & Kazan, Y. (2010). Mechanical characterization of matrix coarse-grained soils with a large-sized triaxial device. *Can. Geotech. J.* **47**, (4) 425–438.

Simo, J.C. , Hughes, T.J.R., 1998. *Computational inelasticity*, Springer, New York.

Tamagnini, C., Ciantia, M.O., 2016. Plasticity with generalized hardening: constitutive modeling and computational aspects. *Acta Geotech*. **11**, 595–623.

Thornton, C., Zhang, L., 2010. On the evolution of stress and microstructure during general 3D deviatoric straining of granular media. *Géotechnique* **60**, 333–341.

Wan, R., Pinheiro, M., 2014. On the validity of the flow rule postulate for geomaterials. *Int. J. Numer. Anal. Methods Geomech*. **38**, 863–880.